

Soft Matter

Accepted Manuscript



This is an *Accepted Manuscript*, which has been through the Royal Society of Chemistry peer review process and has been accepted for publication.

Accepted Manuscripts are published online shortly after acceptance, before technical editing, formatting and proof reading. Using this free service, authors can make their results available to the community, in citable form, before we publish the edited article. We will replace this *Accepted Manuscript* with the edited and formatted *Advance Article* as soon as it is available.

You can find more information about *Accepted Manuscripts* in the [Information for Authors](#).

Please note that technical editing may introduce minor changes to the text and/or graphics, which may alter content. The journal's standard [Terms & Conditions](#) and the [Ethical guidelines](#) still apply. In no event shall the Royal Society of Chemistry be held responsible for any errors or omissions in this *Accepted Manuscript* or any consequences arising from the use of any information it contains.

Soft Mode of Charged Chiral Fibrous Viruses (fd)

Kyongok Kang

*Forschungszentrum Juelich, ICS-3, Soft Condensed Matter, Juelich, 52425, Germany.**

(Dated: June 13, 2016)

The frictional forces in the suspensions vary on the size, shape, and the surface of particle, either as charged or neutral. For anisotropic particles of no spatial gradient in order parameter under external parameters, they exhibit either a continuous phase transition or the "freezing" of order parameter fluctuation. They are known as collective soft-mode that has finite cutoff dispersion where the relaxation time diverges. From the microscopic dynamics of charged chiral fd-viruses, the soft mode is revealed with a rotation restoring "twist", obtained from both polarized (VV) and depolarized (VH) small angle dynamic light scattering. Here, I have found the minimum spatial coherence length at a lower I-N binodal concentration that is due to the reverse of electrostatic repulsive forces, as an increase of concentration of charged chiral rods.

PACS numbers: 64.60.-i, 82.70.Dd, 47.20.Hw

I. INTRODUCTION

The control of orientation of domains of ionic impurities and inhomogeneous charged groups of particles under depolarized field are important to improve the switching efficiency of surface stabilized ferroelectric displays and functional panels [1]. Random motions of mobile charged particles and condensed ion-polarizations are expected to occur small, however, not negligible in the fluctuations of collective behavior of local director fields. Dynamic light scattering is a well-used method to measure the collective motions of particles, where the anisotropic macromolecules can be further distinguished by the parallel and perpendicular translations diffusion, as well as the rotational diffusion [2]. In the presence of ionic impurities with a polar type of ferroelectric liquid crystal [1], the electrostatic (Coulomb) interaction is apparent between mobile ions and the director field. Recently, a delicate difference between the self-organization of "condensed" and "uncondensed" F-actin bundles is discussed by the counterion density waves due to multivalent ion concentrations relating to the twist distortion of F-actin helix [3], which is also interesting to the system of charged chiral rods. Brownian dynamics (BD) simulations are shown for a slight deviation between the stiff and flexible chains with- and without-hydrodynamics in the intermediate range of scattering wavevector, in DNA fragments [4], and coil-globule transitions of DNA molecules by a cationic surfactant [5]. In the case of charged particles, cumbersome interactions occur due to either ion specificity or space charges that can form during the change of configurational entropy, shown by electrophoretic light scattering [6], and non-zero mobility variances in heterodyne correlation functions [7].

Interestingly, the repulsive forces between charged col-

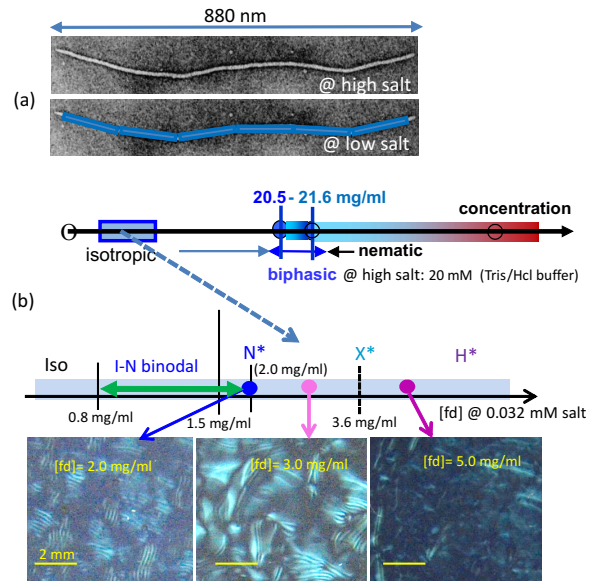


FIG. 1: (a) Simple scheme of the comparison of high (20 mM) and low (0.032 mM) salt of a charged fd-virus. (b) Concentration-dependent phase diagram of both salts, and depolarized optical morphologies (bottom) of the fd-concentration at a low salt concentration of 0.032 mM. Isotropic, I-N (isotropic-nematic) biphasic, N* as a chiral-nematic phase. X* and H* are the hierarchical chiral-mesophases, at higher concentrations.

loids with an electrostatic interaction of ions are shown for salt-free polyelectrolytes with a minimum value of an effective diffusion coefficient [8]. The statistical models of the density and charge fluctuations are considered in two limiting cases; either a dense ionized matter by the small wavevector dependence low frequency spectrums [9], or the elastic moduli in simple fluids for long-wavelength limit [10]. Although, the coupled translational-rotational diffusion are discussed for optically anisotropic biological molecules [11, 12], such as TMV virus [13]-[15], collagen [16], [17], and filamentous viruses (Pfl, M13, and potato virus X) [18, 19], there is no yet experimental realization

*Electronic address: k.kang@fz-juelich.de; URL: http://www.fz-juelich.de/SharedDocs/Personen/ICS/ICS-3/EN/Kang_K.html?nn=543650

of the coupling in the high concentration of charged rods.

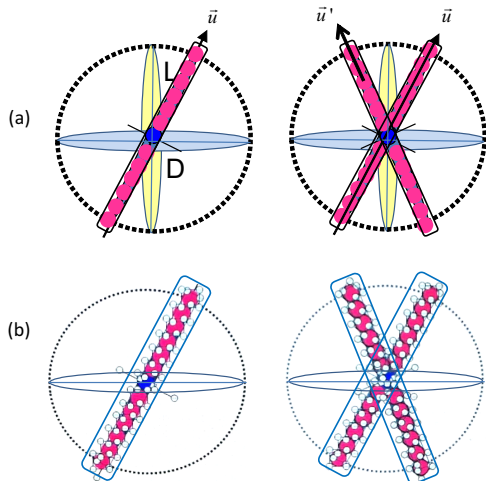


FIG. 2: The brief illustration of an excluded volume effect for (a) hard-core of rods and (b) for charged rods, with the length L , diameter D , and the local orientation of \vec{u} . Lower concentration (of an isotropic phase) and higher concentration (above the isotropic-nematic coexistence) is referred to as left and right in (a) and (b), respectively. At higher concentration, the "twist" effect may play a role in two interacting rods.

Here, in this work, the system is chosen as the crowded suspensions of charged fibrous viruses (fd) at a low ionic strength (of $0.032mM$ salt), where deformations of thick electric double layers are present. The ionic properties of filamentous bacteriophage fd are established by Zimmermann et al [20], where the surface charge of fd-virus is determined by polyelectrolyte titration, as the isoelectric point of a pH- value of 4.2. Also number of ionizable residues (of carboxylated and amide groups) [21] are bounded in bacteriophage fd coat protein and their pKa values are provided in Table in Ref. [20]. The rotational diffusion of fd-virus suspensions for various ionic strengths is tested by the rheological properties at a dilute and intermediate fd-concentration [22], which is related to the intrinsic viscosity of flexible rod-like (cylindrical or ellipsoidal) macromolecular solutions. The rotational diffusion is expected to be rather hindered by an increase of fd-concentration, for two extreme case of salt-free and high ionic strength [23]. So far the structure and dynamics of suspensions of charged rod-like particles are shown in a 'diluted' isotropic phase, by means of dynamical mean-field theory and MC simulation [23, 24]. The pair-distribution of charged fd-rods is then estimated by depolarized structure factor for rods with different rod lengths, and Monte Carlo simulations [25]. However, there is no yet direct evidence of dynamical modes of charged fd-rods, as an increase of fd-concentration at a low ionic strength.

In an equilibrium, when the system exhibits a critical slowing down behavior, on approaching a phase transition, the fluctuations of order parameter lead to a collective soft mode that is shown with a finite cutoff wavevec-

tor in the dispersion relation. This is related to the thermodynamic potential, where the kinetic coefficients are engaged with the inverse of a viscosity [26]. Another feature of an equilibrium behavior is the enhanced order parameter with the spatial coherence length. *It is the aim of this paper to discuss a collective microdynamics of these highly charged fd-rods, by means of small angle dynamic light scattering (in the wavevector ranges of $1-8 \mu m^{-1}$). The spatial coherence length is then obtained from the soft mode that gives different cutoff wavevector, for a given fd-concentration. The change of coherence length is estimated by the collective microdynamics of charged chiral fd-viruses.*

This paper is organized as follows: Section II is consisted of brief background theory and experimental details for collective dynamics, where the small angle dynamic light scattering are performed for given fd-concentrations. With a well-controlled ionic strength (of $0.032 mM$ salt buffer solution), the rod concentration are crowded enough to form several phase transitions; an isotropic-nematic coexistence, a chiral-nematic phase, and hierarchical chiral mesophases. Not only qualitatively different dispersion relations are observed, but also collective soft modes are exhibited for both polarized (VV-mode) and depolarized (VH-mode) light scattering. The sections from III to VI are the relaxation behaviors in dispersion relations, obtained from the dynamic light scattering correlation functions, as an increase of concentration. Finally, concentration-dependent coherence length is provided with a continuous rotation restoring "twist" effect in section VII, followed by conclusion and discussion.

II. BACKGROUND THEORY AND EXPERIMENTAL DETAILS

A. The System: Charged Chiral fd-viruses

Highly charged fibrous virus (fd) suspensions at a low ionic strength are used as a model system for thick charged rods, where dissociation of condensed ions are released to the bulk salt solution, resulting an increase of the effective diameter, and forming thick electric Debye screening length [27]. By increasing an fd-concentration, the system undergoes an isotropic-nematic transition, as well as the formation of orientational textures in chiral-nematic phases, before the structural arrest is reached at a glass transition concentration [28]. Since fd-virus particles carry sufficient amount of negatively charged groups on thin condensed counterion layer, the electrostatic Debye length is tuned by changing the ionic strength of a buffer solution. There are competing interactions between electrostatics and hydrodynamic interaction, such that, above the ionic strength of $1mM$ salt solution, thin electric double layers are present, in which screened hydrodynamics is valid [27], however, below $1mM$ salt solution, relatively larger Debye length is present as com-

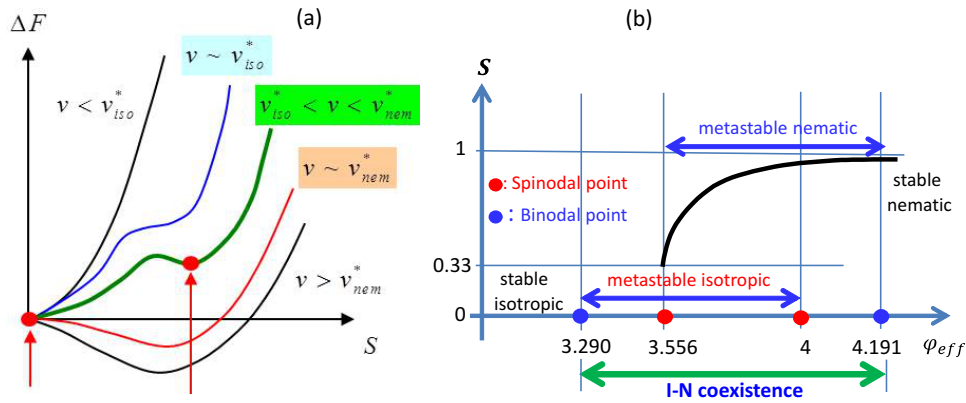


FIG. 3: (a) The free energy difference of rods as a function of order parameter S , and the volume fraction v . Note that there are two steady equilibrium order parameters (red dot points) for the isotropic-nematic (I-N) coexistence concentration that is indicated as the green line. (b) A brief scheme of an equilibrium order parameter S as a function of effective volume fraction, ϕ_{eff} , in which two binodal and spinodal points are indicated.

pared to the bare diameter of fd-virus (of $6.8nm$). Then the electrostatic polarization becomes responsive to the external deformation of thick electric double layers. Current work is done at a low ionic strength of $0.032mM$ salt, where Debye length of fd-virus is about $54nm$, as 7 times larger than the bare diameter, and the length of fd-virus is $880nm$, thus it gives the reduced aspect ratio of 16, shown in **Figure 1a**. The location of binodals and spinodals depend both on the Debye screening length, and the effective number of surface charges [29]. The experimental binodal concentrations are 0.8 ± 0.2 and $1.5 \pm 0.4 mg/ml$ for the $0.032 mM$ buffer. The lower binodal concentrations are in very good agreement, while the experimental upper I-N binodal concentration is slightly higher than the theoretically predicted value. The interest is then what types of collective microdynamics exist for interacting charged fd-rods, by entering an isotropic-nematic binodals, and chiral-nematic phase concentrations. **Figure 1b** is shown the concentration diagram extending above I-N coexistence and up to hierarchical chiral mesophases, with depolarized optical morphologies.

B. Free energy description of an excluded volume effect and order parameter

In the concentrated suspensions of rod-like colloids or polymers, an excluded volume is convenient to facilitate the free energy for a given orientational distribution function, with the sum of all contributing interactions. In order to use free energy description, few basic assumptions are needed as follows; (i) first, a mean-field approach is considered, such that the dynamics of a single particle presents the whole motion of thermal ensemble averages of the system, (ii) the probability to find an orientation in space is the Boltzmann distribution function relating to an interaction energy versus thermal energy, and (iii) there is also a "spontaneous" aligning effect due to an

anisotropic shape, above a certain high concentration, in the absence of an external field. Thus different kinetics of order parameter is expected to occur depending on the volume fractions or effective volumes, as an isotropic, isotropic-nematic coexistence (I-N binodals), and a chiral-nematic phases. **Figure 2** is shown the brief sketch of possible configuration of an effective volume effect for a hard-rod (in **Figure 2(a)**) and a charged rod (in **Figure 2(b)**), where two rods indicating as a higher concentration, in which the pair-wise interaction play a role in some degree of twist elastic deformation of angular distributions between interacting rods. Then whether there will be any different rotational frictions of charged rods, as compared to hard-core rods or not would be an interest of topic. If the orientational distribution function is as $P \sim \exp(-\beta \sum u(i, j))$, where the interaction energy of the particle i and j is $u(i, j)$, and the Boltzmann factor is $\beta = 1/k_B T$, then the free energy is proportional to the logarithmic function of a partition function Ψ ,

$$f(\Psi) \sim V k_B T \left\{ \ln V - 1 + \sum_a \Psi(U_a) \ln \Psi(U_a) \right\}, \quad (1)$$

where V is the volume of the N -particle system. The interaction potential of the system is varied by either a hard-core like-interaction, or soft-potential for charged particles. The rotational motion of rods in both isotropic and nematic phase can be expressed by the kinetics of order parameter tensor as a function of unit director field for two neighboring rod indices as n_α and n_β for

$$S_{\alpha,\beta}(t) = \langle n_\alpha n_\beta - 1/3\delta_{\alpha\beta} \rangle = S_{eq}(n_\alpha n_\beta - 1/3\delta_{\alpha\beta}). \quad (2)$$

The largest eigenvalue of an order parameter tensor gives the equilibrium order parameter, S , as $\partial S/\partial t = -6D_r \{ \partial f / \partial S \}$, where D_r is the rotational diffusion constant [30]. As one can see in the **Figure 3a**, the volume fraction v is in the isotropic-nematic phase coexist, i.e., $v_{iso} < v < v_{nem}$, two equilibrium order parameters are found (indicated as two red dot points).

Depending on the volume fraction, different free energy deviations are expected as a function of order parameter S . Furthermore, the effective surface potential of charged fd-rods, experimentally found order parameter, can be varied with some scaling parameter for different ionic strength as a function of effective volume fraction [27]. The most general equation of motion for the order parameter tensor, \mathbf{S} , is expressed as the sum of three contributions, as

$$\frac{\partial \mathbf{S}}{\partial \tau} = \Delta_{id} + \Delta_{Q,hc} + \Delta_{twist}, \quad (3)$$

with the dimensionless time variable, $\tau = D_r t$, where D_r is the free rotational diffusion coefficient. The various contributions are as follows: First term, Δ_{id} is the contribution from free diffusion,

$$\Delta_{id} = 6 \left[\frac{1}{3} \hat{\mathbf{I}} - \mathbf{S} \right], \quad (4)$$

where \mathbf{I} is the unit tensor. The second contribution $\Delta_{Q,hc}$ comes from interactions, unperturbed by the external field, with an effective hard-core diameter that accounts for the above discussed electrostatic interactions, as indicated by the subscript "Q",

$$\Delta_{Q,hc} = \frac{9}{2} \frac{L}{d_{eff}} \varphi_{eff} \{ \mathbf{S} \cdot \mathbf{S} - \mathbf{S} \mathbf{S} : \mathbf{S} \}, \quad (5)$$

with an effective diameter d_{eff} that can be expressed by an effective dimensionless concentration $(L/d_{eff}) \varphi_{eff}$ [31, 32]. The following expression for the effective diameter can be derived,

$$d_{eff} = \kappa^{-1} [\ln K_Q + \gamma_E], \quad (6)$$

where κ^{-1} is the Debye length and $\gamma_E = 0.5772 \dots$ is Euler's constant, and where,

$$K_Q = \frac{2\pi \exp\{\kappa d\}}{(1 + \frac{1}{2}\kappa d)^2} \frac{l_B}{\kappa L^2} (N_0 - N_{c,0})^2, \quad (7)$$

with d , as the core diameter, l_B , the Bjerrum length, N_0 , the number of immobile charges chemically attached to the surface of a rod, and $N_{c,0}$ the number of condensed ions of a rod in the absence of any electric fields [29]. The third contribution Δ_{twist} is the twist contribution, which turned out to be not negligible parameter for charged fd-rods, where thick electric double layers are present [31, 32],

$$\Delta_{twist} = -\frac{9}{2} \left[\frac{5}{4} - \ln 2 \right] \frac{1}{\kappa d_{eff}} \frac{L}{d_{eff}} \varphi_{eff} \{ \mathbf{S} \cdot \mathbf{S} - \mathbf{S} \mathbf{S} : \mathbf{S} \}. \quad (8)$$

The detailed location of a lower I-N binodal concentration, including the twist effect, can be obtained from the corresponding dimensionless concentration of

$(L/d) \varphi = 3.290 \dots$, as predicted by Onsager [33, 34]. A brief scheme of I-N binodal and spinodal points are depicted in **Figure 3b**. This relies on the fact that the charge-charge interactions as well as the twist effect have the same functional dependence on the orientational order parameter tensor in the equation of motion (3). The lower binodal concentration is set by,

$$\left[\frac{L}{d_{eff}} \varphi_{eff} \left\{ 1 - \left[\frac{5}{4} - \ln 2 \right] \frac{1}{\kappa d_{eff}} \right\} \right] = 3.290 \dots \quad (9)$$

The same procedure can be used to obtain the location of an upper I-N binodal and two spinodal concentrations. The Onsager value of $(L/d)\varphi$ for the upper binodal is 4.191, shown in **Figure 3b**. Typical steady-state viscosity increases in an isotropic phase, but it decreases in a nematic phase [30, 35], expressed as $\eta = v k_B T / 6 D_r \{ ((1-S)^2 (1+2S) (1+3S/2)) / ((1+S/2)^2) \}$, which is shown as the direct relation of order parameter and rotational diffusion constant, such that the rotational torque is related to the stationary intrinsic viscosity that is resulting order parameter kinetics [36]. Here, the rotational diffusion constant D_r is assumed to be a complete segment rotation of the rod length [37]. Total free energy is then described by the sum of all different contributions of the director field, ion impurities, and the charge core interactions, as well as the coupled ones with these terms. In the case of strong charge core interactions, the director field is equally important, the contributions of ion impurities can be "instantaneously" enslaved by the director field exhibited in the thermal fluctuations that are measurable by dynamic light scattering. Thus random-phase approximation (RPA) is useful to explore intermolecular interactions for the effect of an excluded volume in DLS of charged rods [38, 39]. The collective dynamics of director fluctuations are then further distinguished by the mobilities of ion impurities, relating to the rotational viscosity. The director fluctuations of nematic phase can be then predicted by the superpositions of symmetry restoring variables in long-ranged hydrodynamics, shown with divergence of susceptibility [40].

C. Collective soft mode of relaxation behaviors

The rotational diffusion and intrinsic viscosity for rod-like macromolecules are influenced by the hydrodynamics [2], and thereby for charged colloids, the electro-viscous forces may play an additional role in the elastic deformation of a squeezing flow, shown by a Derjaguin approximation [41]. In particular, the coupling of rotational and translational motions is seen for anisotropic particles with a low frequency VH light scattering [42], where the explicit expression for the VV-VH-scattering intensities [43]. This can be also observed for biological substances, such as motile microorganisms [44], E-coli bacteria [45], and lysozyme [46]. Depending on the aspect

ratio of rods, dynamic structure factor is estimated by the form factor of rods [47]. The example of a dynamic structure factor is reported for living particle motions (of motile or swimming) due to the motility versus "resting" microorganism studied in the scattering spectra [44], but the velocity distribution of these living particles are not a simple Gaussian function. As an increase of concentrations of rods, the strength of intermolecular interactions and different mutual diffusion constant exist in friction coefficients [48]. Thus for a collective motion of homogenous and modulated structure, the system is set by a time-fluctuating spectrum of order parameter that "freeze" at a finite wavevector, by showing the critical slowing down behaviors such that the relaxation rate becomes zero ($\Gamma = 1/\tau = 0$), and the time of relaxation diverges ($\tau = \infty$) at the wavelength at $q = q_c = 2\pi/\xi$ [1]. One of the examples is the Sm-A-Sm-C* transition of thermotropic system of chiral smectic system, where there will be a collective mode: Continuous symmetry breaking exists in chiral Sm-C* phase, while as the symmetry restoring (so-called Goldstone) mode to restore the broken symmetry in Sm-A phase [1, 26]. The spatial coherence length, ξ , is then the characteristic measure of the collective soft mode, depicted by so-called 2nd order phase transitions. However, no yet soft mode is explored in the lyotropic system, where the external parameter can be replaced by the critical concentration, instead of a critical temperature. Also the kinetic process in the vicinity of a phase transition will be related to the inverse of a viscosity of the system. The direct way to investigate the propagation of an order parameter is to measure the relaxation rates (or a damping constant) as a function of wavevector for various concentrations, such that the cutoff wavevector can be estimated with different phase-boundaries.

D. Method: Small Angle Scattered Intensities and Correlation Functions of Polarized (VV), and Depolarized (VH) Dynamic Light Scattering

Structure of small particles can be explored by either scattered light intensities [49] or the real-space small angle light scattering for the particle arrangements [50, 51], where the optical contrast is varied with the shape of scatterers. In this experiment, the range of scattering angle is small, as comparable to the length of a charged rod (as $1 - 8 \mu\text{m}^{-1}$), and preferred directions of alignment occur in the crowded concentrations, persisting orientational motions of charged fd-rods. Home-made small angle vertical dynamic light scattering is used to determine the collective microscopic dynamics of many interacting charged chiral fd-rods, at a low ionic strength (of 0.032mM salt).

Figure 4a is a simple scheme of small angle dynamic light scattering setup [52], where the incident laser beam is vertically mounted to facilitate the horizontally round quartz cylindrical cell, in **Figure 4b**, with the scattering

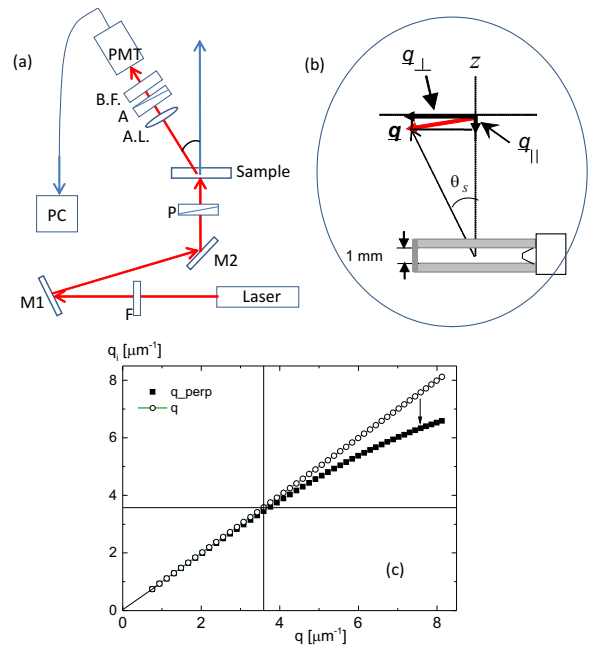


FIG. 4: (a) A brief scheme of the experimental setup of small angle vertical dynamic light scattering: F: filter, M: mirror, P: polarizer, A: analyzer, A.L.: Achromatic lens, B.F: band pass filter. (b) The scattering geometry passing through the sample that is located in the vertical to the incident laser beam ($= 633\text{nm}$). (c) Calibration of scattering wavevector component perpendicular to the incident beam. Note that there is hardly any difference, below the scattering wavevector of $q_c \sim 3.6 \mu\text{m}^{-1}$, but the deviation appears above, indicated as an arrow.

geometry: A 35 mW He-Ne laser (JDS Uniphase Model 1145P series, 633 nm wavelength), which is used as an incident light perpendicular to the cell. Two mirrors are used to align the incident laser beam from bottom to top direction. A rotation stage (NanoRotator, Melles Griot) is used as a goniometer, which is controlled by the software stepper motor controller (advanced positioning technology by Melles Griot 17BSC002). To achieve vertical alignment of the incident laser beam, we have used two pinholes and a photon detector on an optical rail. The scattered light is then collected through an optical fiber that is connected to an avalanche photo diode detector. We use an ALV-5000/EPP multiple tau digital real time correlator (by ALV-GmbH, Langen, Germany), which computes photon correlation functions with a linear time-step distribution with time lags between $0.125 \mu\text{s}$ and 2147s . The optical fiber is placed on an arm that is connected to the goniometer. An essential element of this vertical DLS is the achromatic lens (with a focal length 75 mm) that is placed on the detection side, to ensure that the scattering volume that is probed is well within the bulk of the sample. Without this lens, it turned out that the measured correlation functions exhibit spurious long-time relaxation.

The incident beam is straight up to the 1mm thick

sample cuvette, and the detector photomultiplier (PMT) collects the scattered laser light intensity by varying the goniometer angle of $5 - 50^\circ$ (as the scattering wavevector range of $1 - 8 \mu\text{m}^{-1}$). Then the scattering wavevector can be decomposed either as perpendicular or parallel to the incident beam. When the scattering angle is small, the perpendicular component of the scattering wavevector is dominant below the wavevector of $q \sim 3.6 \mu\text{m}^{-1}$ (i.e., the scattering angle of $20 - 22^\circ$), shown with the comparison to the total wavevector, depicted in **Figure 4c**. However, at higher wavevectors, perpendicular component itself is deviated from the total scattering wavevector, due to a slight contribution from the parallel component of the wavevector.

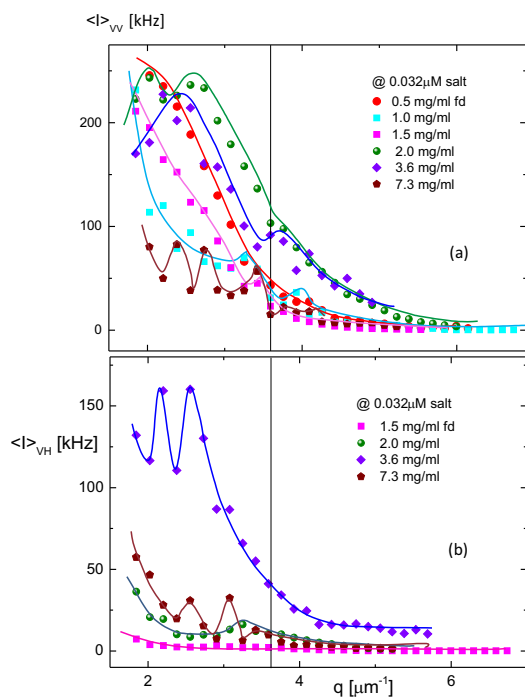


FIG. 5: The averaged scattered intensity as a function of wavevector for (a) polarized VV-mode and (b) depolarized VH-mode. As one can see below the wavevector of $q \sim 3.6 \mu\text{m}^{-1}$, above isotropic-nematic binodal concentration, the strange peaks are appeared in the averaged intensity.

Prior to the details, the overall measured scattered intensities of polarized light (VV-mode) are shown in **Figure 5a**, as a function of fd-concentration, as well as the depolarized light scattering intensity (of VH-mode) in **Figure 5b**. The black vertical line indicates at the wavevector of $q \sim 3.6 \mu\text{m}^{-1}$, which distinguishes the perpendicular (at below the value), and parallel component. Much complicated scattered intensity distributions are shown in both VV- and VH-modes, below the q -value, as the perpendicular components, at a low ionic strength (of $0.032mM$). Within the lower wavevector limit, interestingly, different features of scattered in-

tensities are seen. In VV-mode, for an isotropic-phase (of 0.5 mg/ml), standard scattered intensity distribution is shown, however, as an increase of concentration (as isotropic-nematic coexistence concentration range of $1.0 - 1.5 \text{ mg/ml}$), the distribution have changed, and eventually there are two pronounced intensity peaks are shown at chiral-nematic phase (of concentration 2.0 mg/ml). Thus, this concentration can be remarked as approaching the chiral-nematic phase, and whether there will be a concentration-dependent form factor relating the nematic-chiral-nematic state would be then left as an open question. Also pronounced VH-mode are shown the concentration, above the isotropic-nematic coexistence concentration, and the highest scattered intensity distributions are shown with two pronounced peaks in above chiral-nematic phase (as 3.6 mg/ml), which suggests that more rotational motions are probable.

The normalized intensity-intensity autocorrelation functions are provided for few low finite wavelengths that are comparable to the inverse of a persistence length of fd-virus particle ($2.2 - 2.8 \mu\text{m}^{-1}$) in **Figure 6**: First of all, disregard of various concentrations, two dynamical modes are evident in the measured intensity autocorrelation functions of both VV-mode (**Figure 6a**) and VH-mode (**Figure 6b**). Rather complicated decays in depolarized VH-mode indicate the intra-particle interactions due to the interactions of order parameter coupled to the concentration.

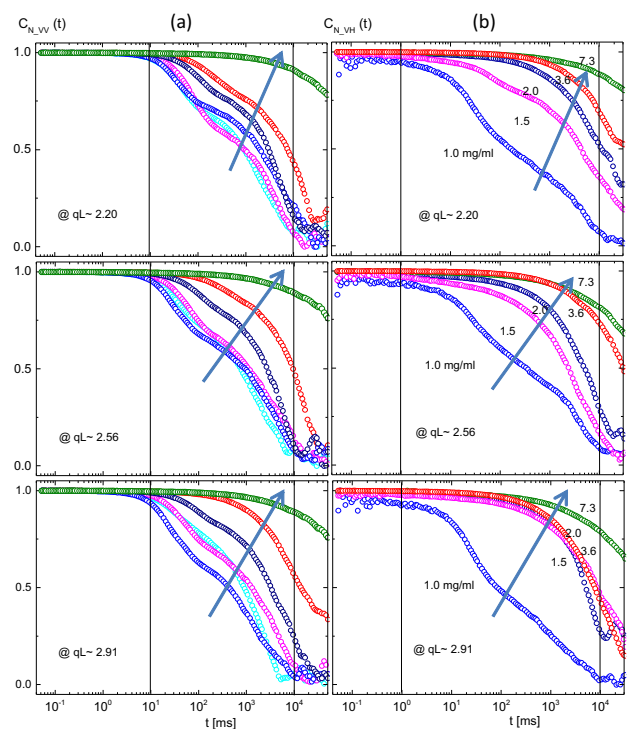


FIG. 6: Normalized correlation functions of fixed few low wavevectors, comparable to the persistence length of charged fd-rods for (a) polarized VV- and (b) depolarized VH-scattering. The arrow indicates the increase of a fd-concentration.

Rather complicated decay functions of the depolarized (VH) dynamic light scattering, measured at the wavelength corresponding ranges of the persistence length of fd-virus particles ($2.20 \mu\text{m}^{-1} < qL < 2.91 \mu\text{m}^{-1}$), are much stretched in the concentration of 1.0 mg/ml, in **Figure 6b**. This indicates either polydispersity or the coupled motions of rotations and translations. From the current measurement of the phase-diagram at this low ionic strength (of 32uM salt), the 0.8-1.5 mg/ml is isotropic-nematic coexistence, and above 1.5 mg/ml, there is a chiral-nematic phase. The difference of the nematic- and chiral-nematic is turned out to be the flow kinetics, where nematic-flow is much ($\sim 100\text{times}$) faster than the chiral-nematic phase. That is the reason why the VH-correlations are slow down enormously at above 1.5 mg/ml in **Figure 6b**.

The fits of these correlation functions are provided with the fast- and slow-dynamical mode in the following sections (of III-VI): The appearance of a slow decay mode is a feature of the coupling of rotational and translational anisotropic diffusions [39], resulting from the deviation from the perfect rigid-rod model, likewise observed in higher concentrations of PBLG solution[53]. Another aspect of a slow mode is the cooperative motion relating to charge dissociation/ association for charged fd-rods (at a low ionic strength). When the system has strong interactions of neighboring charged rods, the electrostatic interaction is presented with an effective diameter of rod that varies with a salt concentration, via Debye length, as well as the virial expansion relating to the Donnan membrane equilibrium [54]. Although the effect of ionic strengths on short-DNA rods and diluted suspension of fd-rods are tested by a quasi-elastic light scattering before [55]-[57], this is the first time to observe the collective microscopic dynamics of charged chiral fd-rods, in crowded system revealing a delicate electrostatic interaction between short-ranged attraction and long-range repulsion.

III. RELAXATION BEHAVIORS OF AN ISOTROPIC PHASE

When the concentration is low as an isotropic phase, the orientational order is random with no preferred direction in the averaged director field. The scattered intensity of VV-polarized light in **Figure 7a**, is shown with a function of wavevector, as expected distribution for a rod-shape of macromolecules. Note that, here, relatively shorter range of the wavevector ($1 - 8 \mu\text{m}^{-1}$) is probed as compared to the wavevector of Konstanz group (as $10 - 30 \mu\text{m}^{-1}$)[58]. Only VV-polarized light intensity signal is observed with raw intensity auto-correlation functions in **Figure 7c, d**, in the relaxation behaviors of an isotropic phases: where the arrow indicates an increase of a wavevector, below $q \sim 3.6 \mu\text{m}^{-1}$ and above $q \sim 3.6 \mu\text{m}^{-1}$, respectively. At very low amplitudes, while the slow mode is not pronounced with an increase of wavevec-

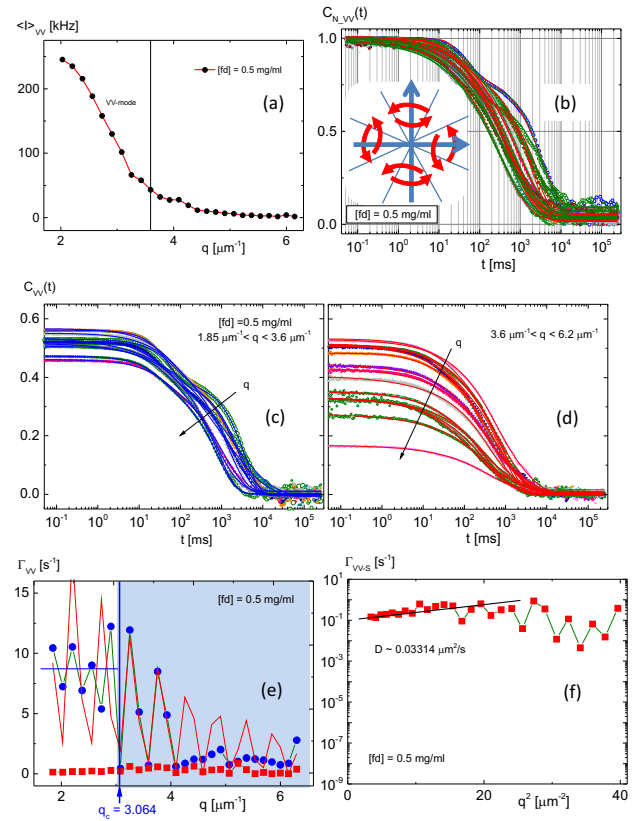


FIG. 7: (a) The averaged scattered intensity of an isotropic phase (fd-concentration of 0.5 mg/ml), with a pronounced scattered intensity below the scattering wavevector of $q \sim 3.6 \mu\text{m}^{-1}$. The black lines are indicated to the corresponding to the wavevector of $q \sim 3.6 \mu\text{m}^{-1}$. (b) The normalized correlation functions of polarized VV-mode for an isotropic phase. (c) Raw intensity auto correlation functions for below the scattering wavevector of $q \sim 3.6 \mu\text{m}^{-1}$, and (d) above the wavevector. (e) Dispersion relations of an isotropic phase for fast- and slow-mode in VV-scattering, where the red line in fast VV-mode is the damping motion. (f) Detailed view of slow mode of VV-scattering of (e), with a rough estimation of diffusion constant.

tor. In the normalized correlation functions of **Figure 7b**, the lines are fitted with two dynamical modes; one is fast-mode that is related to parallel to the rod, and the other is slow-mode due to the perpendicular direction of thermal fluctuations. The empirical fitting function is used as $g_2(t) - 1 = B + A_f \exp(-2\Gamma_f t) + A_s \exp(-2(\Gamma_s t)^\beta)$, where Γ , A , and B is the relaxation rate (or a damping constant), amplitude, and background, respectively.

The stretching exponents are found to be as $0.5 < \beta < 1$ for extending long time tails in the correlation functions. The inset of **Figure 7b** is shown a brief illustration of the possible configuration of two interacting charged fd-rods in an isotropic phase, where two blue orthogonal arrows indicate translational motions in parallel and perpendicular, while as the red curves for random orientations that are equally probable between two orthogonal axes. From the fits, dispersion relations of an

isotropic concentration are obtained in **Figure 7e**, for both fast- and slow-mode, as blue and red data points, respectively. There is a sudden drop of the relaxation rate, Γ_{VV} , of the fast mode (in blue data) in the dispersion relations of an isotropic concentration, seen as the cutoff wavevector of $q_c = 3.064 \mu\text{m}^{-1}$ in **Figure 7e**. This is an indication of the soft mode, disregard of local peaks in the small wavevector. In order to implement the damping motion of a fast mode in VV-scattering, a rough estimation of damping is depicted as $50[\cos(6q - 0.25\pi)]^2 e^{-0.45q}$, as the red line in the fast mode of **Figure 7e**. Note, here, two independent processes are related; one is the cosine oscillating part with an amplitude and the other is an exponential decay. The reason for a decrease of relaxation rates in the fast mode of an isotropic phase is due to fact that there is mainly no preferred director orientation, as symmetric scatters in thermal fluctuations. The hindered motion of mobile ions are partly probable in the fast-mode thermal fluctuation parallel to an increase of wavevector. However, thermal fluctuations at higher wavevectors are overdamped, which also opens the discussion on linear stability of the migration of ions in the electrolyte solution, shown as the shape of scattered intensity at low wavevectors, in **Figure 5**. It is probable that non-zero off diagonal diffusion coefficients due to migration of ionic particles [59], may be relevant to the charged fd-rods that are surrounded with thick electric double layers of mobile ions. Thermal fluctuations of the slow mode, even in the parallel component, are much smaller relaxation rates of perpendicular motions, shown as in the logarithmic scale of a square of wavevector, in **Figure 7f**. The slope of dispersion relation gives a rough estimation of the diffusion constant of a slow mode as $D = \Gamma/q^2$, which is far (~ 100 times) slower than the colloidal diffusion), at low wavevectors. Although it is rather noisy, the relaxation becomes flattened at higher wavevectors. The overall possible decrease of relaxation rate is the electroviscous friction that engaged with a static value of intrinsic viscosity, decreasing with a logarithmic function of an aspect ratio [36], so that the rotational diffusion is predicted to be much influenced by a large aspect ratio. The interpretation of the slow mode will be dealt separately, due to an increase of interaction, with an increase of fd-concentration in following sections.

IV. RELAXATION BEHAVIORS OF ISOTROPIC-NEMATIC BINODAL PHASES

As an increase of concentration of charged fd-rods, nematic phase can coexist with an isotropic phase, so-called an isotropic-nematic (I-N) coexistence, as I-N binodals, seen in **Figure 1** and **Figure 3b**. Theoretically predicted I-N coexistence concentration regions are $0.66 < [fd] < 0.84 \text{ mg/ml}$ and the experimental I-N binodal concentrations are 0.8 ± 0.2 and $1.5 \pm 0.4 \text{ mg/ml}$ for the ionic strength of 0.032 mM buffer [29].

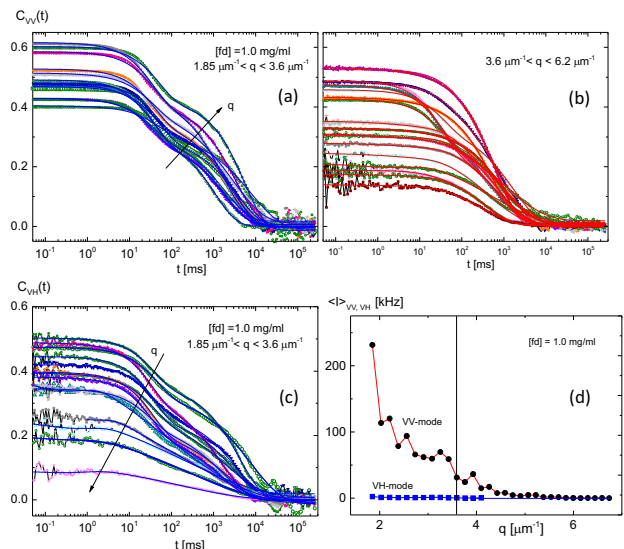


FIG. 8: The raw intensity auto correlation functions of polarized VV-mode (a, b) and depolarized VH-mode (c) for a lower lower isotropic-nematic (I-N) phase (of fd-concentration of 1.0 mg/ml): (a) below the scattering wavevector of $q \sim 3.6 \mu\text{m}^{-1}$, (b) above the wavevector in VV-mode, and (c) below the $q \sim 3.6 \mu\text{m}^{-1}$ in VH-mode, limited for small wavevectors. (d) The averaged scattered intensity of VV- and VH-mode as a function for the wavevector for a lower I-N binodal fd-concentration.

A. Relaxation behaviors of a lower I-N binodal phase (1.0 mg/ml)

As far as the concentration is higher than an isotropic phase, by entering a lower I-N binodal concentration (of 1.0 mg/ml), shown in **Figure 8c,d**, vivid VH-signal is detected systematically, resulting VH-correlation functions only at limited values of lower wavevectors. The signal to noise ratio (or the field amplitude) of VH-scattering is decreased by an increase of a wavevector, stronger stretched slow mode are shown in VH-scattering (indicated as the arrow in **Figure 8c**). The VV- and VH-correlation functions of lower wavevectors are shown in **Figure 8a,c**, respectively. Similarly to the isotropic phase in earlier section, such that evidently higher amplitude of visible two modes are extended to somewhat larger wavevectors. This means more perpendicular thermal fluctuations are available than that of the isotropic phase (see few VV-correlation functions in **Figure 8b**). The normalized correlation functions for both VV- and VH-scattering are shown in **Figure 9a,b**, where the possible configurations of two interacting charged fd-rods are illustrated in the inset of the figures: Translational motions of parallel (in faster time window) and perpendicular (slower time) alignments are shown in **Figure 9a**, while as the rotational motions are shown as red curves in the inset of **Figure 9b** of VH-scattering. The solid lines are the fits with a fitting function of two dynamical modes, here the fast mode is related to the fluctuations

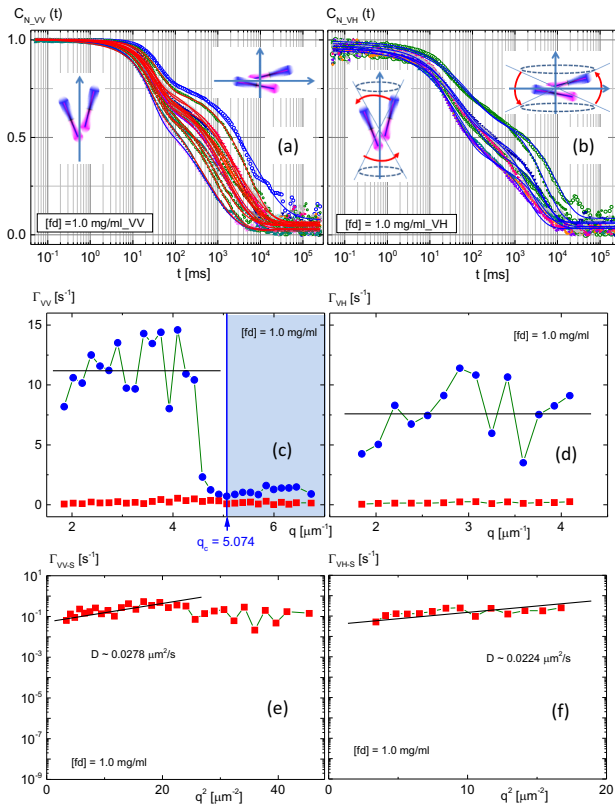


FIG. 9: The normalized correlation functions of (a) polarized VV-mode and (b) depolarized VH-mode for a lower binodal phase (fd-concentration of 1.0 mg/ml). The solid lines are the fits with a fitting function of two dynamical modes, where the fast mode is the parallel, and the slow mode is the perpendicular to the director. The inset is shown a brief illustration for possible configuration of two interacting charged fd-rods. Blue arrow indicates translational motions, and the red are for rotational motions. (c) and (d) are dispersion relations for a lower binodal phase of polarized VV-mode (fast and slow mode), and depolarized VH-mode (fast and slow mode), respectively. (e) and (f) are details of the slow modes, shown in (b) and (d), respectively.

of parallel to the director, and the slow mode is for the perpendicular direction of the alignment.

The corresponding relaxation rates are plotted as a function of wavevector in **Figure 9c** for VV-correlations, where a cutoff wavevector at $q_c = 5.074 \mu\text{m}^{-1}$ is indicated, as the relaxation rate becomes zero in the fast-mode of VV-light scattering. The relaxation rates for VH-correlations are provided in **Figure 9d**. The slow modes for both VV- and VH-correlations are shown in **Figure 9e,f**, respectively. The diffusion constants are found only for the slow modes, slightly smaller than that of the isotropic phase, as the diffusion constants of $D = 0.0278 \mu\text{m}^2/\text{s}$ and $D = 0.0224 \mu\text{m}^2/\text{s}$ for VV- and VH-scattering, which are lower than that of the isotropic phase ($D = 0.03314 \mu\text{m}^2/\text{s}$). There is an averaged non-zero intercept value for the rotational diffusion of $10/6 \sim 1.7 \text{ s}^{-1}$ (in VH-mode), as lower than the

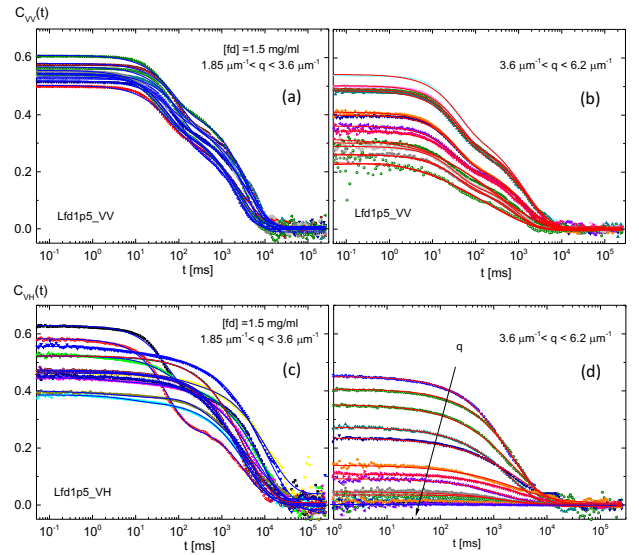


FIG. 10: The intensity auto correlation functions for polarized VV-mode (a, b) and depolarized VH-mode (c, d) for an upper I-N binodal phase (fd-concentration of 1.5 mg/ml).

rotational diffusion constant (of 10 s^{-1}) at a high ionic strength [22].

B. Relaxation behaviors of an upper I-N binodal phase (1.5 mg/ml)

At an upper I-N binodal concentration (of 1.5 mg/ml), the intensity correlation functions and normalized correlation functions are shown in **Figure 10**, and **Figure 11a,b**, respectively. Two dynamical modes are visible at higher wave vector VV-correlations, with somewhat more stretched in slow mode of **Figure 10b**, and wider q -range in VV-mode than a lower binodal concentration. Now VH-correlation functions are not only shown a severe change of amplitude at lower wavevectors, in **Figure 10c**, but also extend to higher wavevectors in **Figure 10d**. However, the fast mode are relatively limited at lower q -range in VH-mode. The inset of normalized correlation, in **Figure 11b**, is illustrated a possible configuration of both rotation and translation in VH-mode with some degree of rotations. The uniqueness of a dispersion relation for this upper I-N binodal concentration is the appearance of a series of discontinuous jump state as an increase of relaxation rate (in **Figure 11c**) in the fast mode of VV-scattering. Also the red line on the fast mode in the VV-scattering of (**Figure 11c**) presents the damping motion of as $[\cos(6q)]^2 e^{0.45q} + 2q$: Here, the additional term of $2q$ is added to the damping motions, with a small step of an increase of shifting wavevector. On the contrary, in VH-scattering, there is an existing soft mode at a cutoff wavevector of $q_c = 2.208 \mu\text{m}^{-1}$ in **Figure 11d**, suggesting that the overdamped motions are present in the depolarized VH-scattering, not a polarized VV-scattering at an upper I-N binodal concentra-

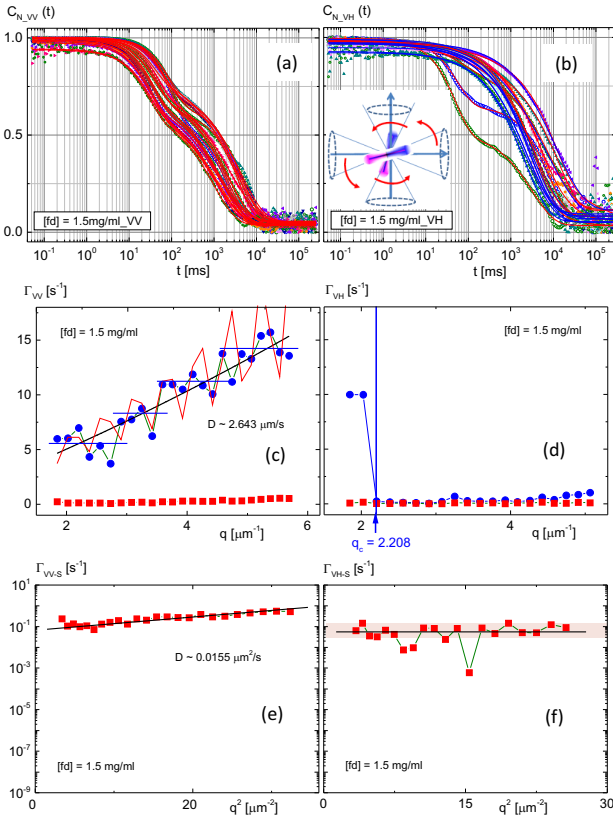


FIG. 11: The normalized correlation functions of polarized VV-mode (a) and depolarized VH-mode (b) for an upper I-N binodal phase (fd-concentration of 1.5 mg/ml). The inset drawing in VH-mode in (b) is indicated for the possible alignments of the charged fd-rods in bulk. (c) and (d) are dispersion relations for an upper I-N binodal phase of fast- and slow-mode of polarized VV- and depolarized VH-scattering, and the details of slow mode are in (e) and (f), respectively. The red line in the fast mode of (c) is depicted of the damping motion.

tion, which is evidently different relaxation behavior, as compared to that of a lower I-N binodal concentration (see **Figure 9c,d**). The dispersion relation of VV-mode is then averaged as the linear in a wavevector, in **Figure 11c**, indicating that a slightly ordered phase is found in diffusive motion, as expected with an anisotropic diffusion constant: The system has indeed shown a reasonable diffusion consonant in VV-mode at the upper I-N binodal concentration (of 1.5 mg/ml), estimated diffusion constant of fast-mode is $D = 2.643 \mu m^2/s$, as a typical colloidal diffusion constant. More aligned thermal fluctuations of director fields are seen in the translational motion. The diffusion constant for a slow-mode in VV-scattering is obtained as slow as $D = 0.0155 \mu m^2/s$. Although the cutoff wavevector is not appeared in the fast mode of VV-scattering, a soft mode exists at a finite cutoff wavevector of VH-scattering (blue data in **Figure 11d**). Since hardly any diffusion is seen in the slow modes of VH-mode, with a complete flattening in **Figure 11f**, the overdamped rotations exist in the dispersion re-

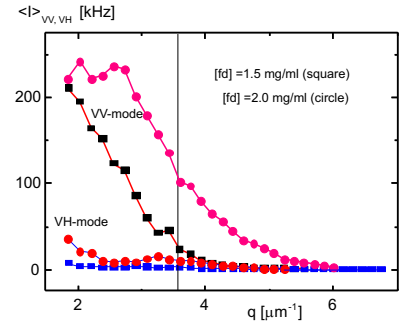


FIG. 12: The averaged scattered intensity of VV- and VH-mode as a function of the wavevector for two comparable fd-concentration: an upper I-N binodal concentration (of 1.5 mg/ml), and a chiral-nematic phase concentration (of 2.0 mg/ml). Note that pronounced scattered intensities and the broadening of intensity peaks, below the scattering wavevector of $q \sim 3.6 \mu m^{-1}$.

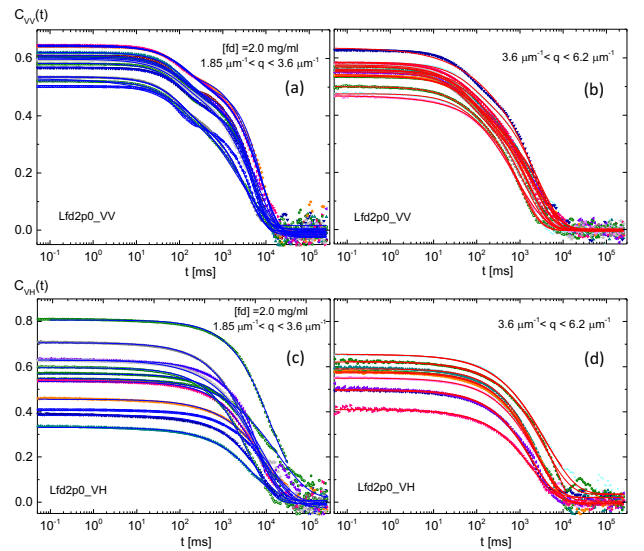


FIG. 13: The raw intensity auto correlation functions of polarized VV-mode (a,b) and depolarized VH-mode (c,d) for a chiral-nematic phase of fd-concentration of 2.0 mg/ml.

lation of VH-mode in this upper binodal concentration. Whether the slow mode in depolarized VH-scattering is related to long-ranged hydrodynamics nematic director fluctuations or not would be another open question[40].

V. RELAXATION BEHAVIORS OF A CHIRAL-NEMATIC PHASE

A fully nematic concentration is in a sense a chiral-nematic phase, since forming a chiral-nematic texture, at the concentration of 2.0 mg/ml for a given low ionic strength. The comparison of scattered intensities (of both VV- and VH-mode) for two comparable fd-concentrations are shown in **Figure 12**; an upper I-N binodal (as 1.5 mg/ml), and a chiral-nematic concentra-

tion (2.0 mg/ml). The overall scattered intensities of VV-signals are detected higher than that of VH-signals, in the I-N coexistence concentrations (in **Figure 12**). Not only more increased scattered intensity of VH-signal is detected at a fully-nematic (as a chiral-nematic) phase (with a concentration of 2.0 mg/ml), but also the shape of intensity broadening is depicted in terms of two separable peaks, in **Figure 12**. As soon as approaching the chiral-nematic, N^* -phase the microscopic dynamics becomes enormously slowing down, due to the existence of orientational textures that are persisted in the chiral-nematic domains, as well as in the helical domains at hierarchical chiral-mesophases (above 3.5 mg/ml). So only it is valid for lower than the upper isotropic-nematic (I-N) binodal concentration (of 1.5 mg/ml), decent distinguish between translational and rotational diffusion is possible in the charged chiral fd-rods. Above the upper binodal concentration, not only the coupling of rotational motion to translation becomes dominant, but also the appearance of increased "twist" interaction or the rotational motions of charged fd-rods.

The correlation functions of both VV- and VH-scattering are provided in **Figure 13**, where pronounced signal-to noise ratio of the VH-signal is detected. **Figure 14a,b** are shown the normalized correlation functions with possible schemes of rotational motions. Constrained field amplitudes are seen in the faster time window of both VV- and VH-correlation functions, implying that the translational motion in parallel is less present than the perpendicular motions. However, the rotational motions are rather broadened in the wavevector.

Also the dispersion of fast-mode in VV- and VH-scattering in **Figure 14c,d**, are shown with the quadratic relation of a wavevector, as it is a diffusive motion. Here, again, the collective soft-mode is exhibited in the fast mode of VV-scattering, as the cutoff wavevector of $q_c = 4.086 \mu\text{m}^{-1}$, in **Figure 14c**, slightly smaller than the cutoff wavevector of $q_c = 5.074 \mu\text{m}^{-1}$ for the lower I-N binodal concentration (in **Figure 9c**), indicating that the dynamic coherence length becomes larger. The red line in the fast mode of **Figure 14c** for the VV-scattering is for the damping motion of $25[\cos(5q - 0.85\pi)]^2 e^{-0.40q}$, interestingly, in which the amplitude of oscillation at an upper binodal concentration is reduced to a half-smaller value of the lower I-N binodal concentration. Also the slope of dispersion relation has a different sign, as the relaxation behaviors are reversed in the fast-mode, between VV- and VH-scattering for the chiral-nematic phase concentration. The flattening in the dispersion of VV-fast mode is somewhat broadening as $q_c = 4.086 \mu\text{m}^{-1}$, shown in **Figure 14c**. The soft mode is now shifted to a zero-wavevector limit, in the fast VH-mode, implying the spatial coherence length becomes sufficiently larger. Here, the formation of orientational textures in the charged fd-rod suspensions is regarded to the length scale, either an optical pitch of the chiral-nematic phase (of $10 \mu\text{m}$) or the persistence length of fd-viruses (as $2.2 - 2.8 \mu\text{m}$) or not would be another interest. The

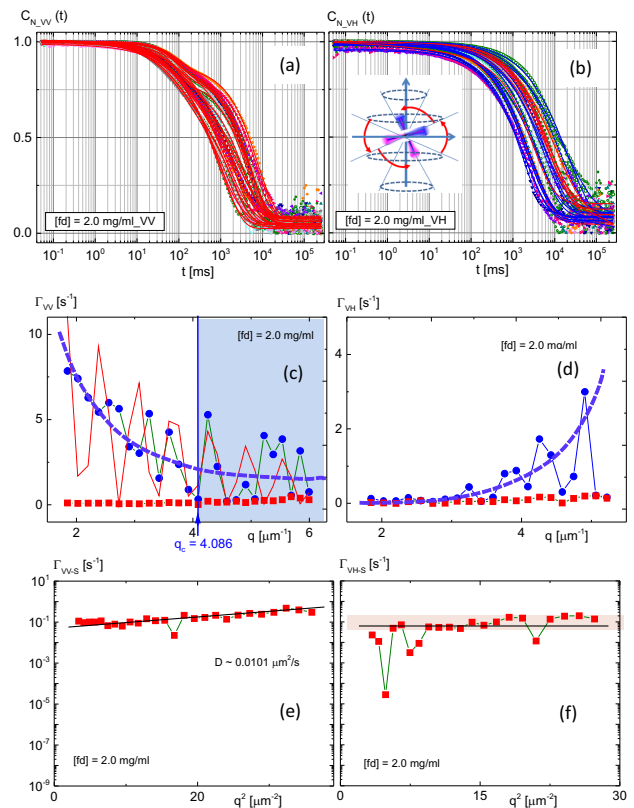


FIG. 14: The normalized correlation functions of (a) polarized VV-mode and (b) depolarized VH-mode for a chiral-nematic phase of fd-concentration of 2.0 mg/ml . (c) and (d) are dispersion relations for fast- and slow-mode of polarized VV-scattering, and depolarized VH-scattering, and the details of slow mode with the diffusion constant are in (e) and (f), respectively. The red line in the fast mode of (c) is depicted of the damping motion.

slow mode diffusion in VV-scattering of **Figure 14e** is $D = 0.0101 \mu\text{m}^2/\text{s}$, as lower than the value of an upper I-N binodal concentration. However, for VH-scattering, more or less averaged relaxation rate is observed as flat in the chiral-nematic phase (**Figure 14f**).

VI. ROTATION RESTORING TWIST OF HIERARCHICAL CHIRAL-MESOPHASES

Now two higher concentrations of hierarchical chiral mesophases are chosen for fd-concentrations of 3.65 mg/ml (distinguished as X^* -phase, based on the depolarized optical morphologies) and 7.3 mg/ml (as H^* -phase). At these higher concentrations, the system is expected to be equilibrated at much long waiting times, exhibiting to significant slow relaxation of orientation textures [28, 60]. At a low wavevector regime, VH-scattering, in **Figure 15**, scattered intensity distributions for two comparable high concentrations of hierarchical chiral-mesophase are not only increased, but also substantially different shapes in the perpendicular direction.

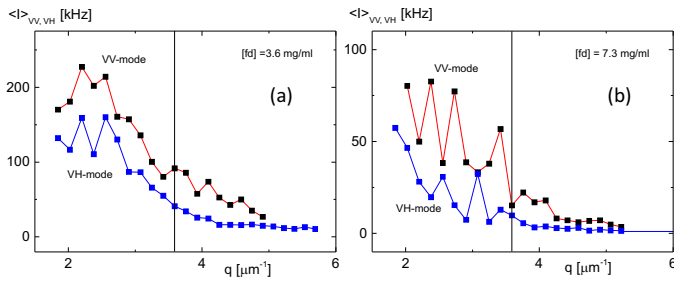


FIG. 15: The averaged scattered intensity of hierarchical chiral mesophases for fd-concentration of (a) 3.6 mg/ml , and (b) 7.3 mg/ml . Note that pronounced scattered intensities below the scattering wavevector of $q \sim 3.6 \mu\text{m}^{-1}$, and substantial increase of the averaged scattered intensity of VH-scattering.

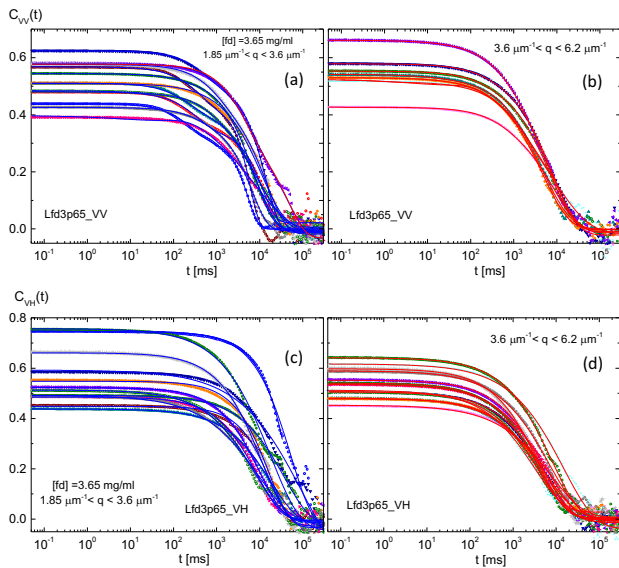


FIG. 16: The raw intensity auto correlation functions of polarized VV-mode (a,b) and depolarized VH-mode (c,d) for a hierarchical chiral mesophase phase (of fd-concentration of 3.6 mg/ml).

For a fd-concentration of 3.65 mg/ml , the intensity correlation functions and normalized correlation functions are shown in **Figure 16**, and **Figure 17a,b**, respectively. The "broadening" of rotational motions are depicted in the inset of **Figure 17b**, in overall correlation functions, for dominant rotational motions along the perpendicular to the rods, except few extended correlation functions at low wavevector in VV-scattering (**Figure 16a**). The dispersion relations of relaxation behaviors of VV- and VH-scattering are summarized in **Figure 17c,d**, for a fd-concentration of 3.65 mg/ml (as X*-phase), where the slow mode for both VV- and VH- are "completely" overdamped, with no indication of the slope in dispersion relations in **Figure 17e,f**. Interestingly, there is a still collective soft mode observed in the fast mode VV-scattering with a cutoff wavevector of $q_c = 2.903 \mu\text{m}^{-1}$, in **Figure 17c**, as a quadratic decrease of the wavevector.

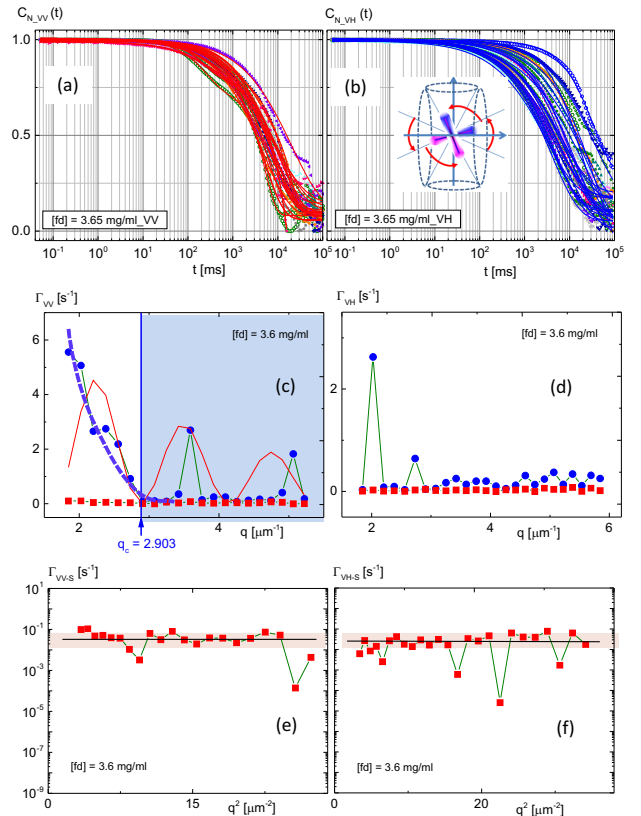


FIG. 17: The normalized correlation functions of (a) polarized VV-mode and (b) depolarized VH-mode for a hierarchical chiral mesophase (fd-concentration of 3.6 mg/ml). (c) and (d) are dispersion relations for fast- and slow-mode of polarized VV-scattering, and depolarized VH-scattering, and the details of slow mode are in (e) and (f), respectively. The red line in the fast mode of (c) is depicted of the damping motion.

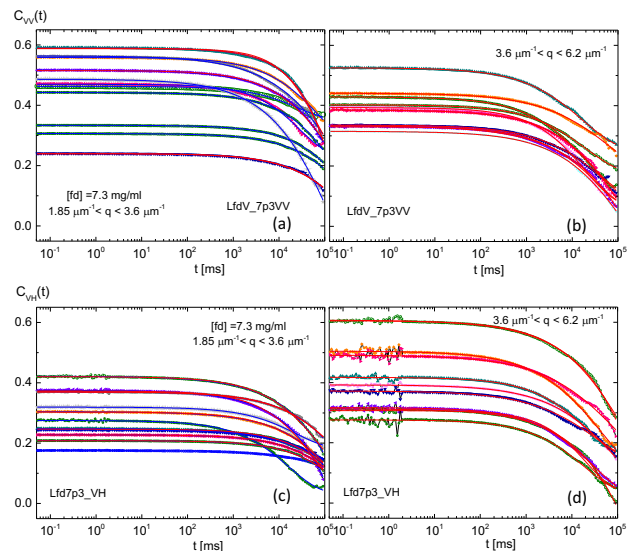


FIG. 18: The raw intensity auto correlation functions of polarized VV-mode (a,b) and depolarized VH-mode (c,d) for a hierarchical chiral mesophase phase (of fd-concentration of 7.3 mg/ml).

The damping motion of a fast mode in VV-scattering is added as the red line on **Figure 17c**, as $10[\cos(2.5q - 2.8\pi)]^2 e^{-0.35q}$, with a lower amplitude. This concentration is then unique to observe the system is now reached to such that damping of translation is occurred in the fast component of the fluctuations. By doubling the concentration, as 7.3 mg/ml (as H*-phase), much severe slowing down behaviors are seen in both measured and normalized correlation functions in **Figure 18**, and **Figure 19a,b**, respectively. The possible configuration of interacting rods is more crowded with randomized rotations with enhanced slowing down behaviors. In the dispersion relation of higher concentration (7.3 mg/ml) of a hierarchical chiral-mesophase of **Figure 19c,d**, the minimal estimation of a soft mode is reached to the lowest q-value in experiment, as $q_c = 1.828 \mu\text{m}^{-1}$. The red line on **Figure 19c** in the fast mode in VV-scattering is the simulated damping motion of $3[\sin(6q - 0.58\pi)]^2 e^{-0.88q}$, which is qualitatively consistent with a decreased amplitude of damping motion, as an increase of charged fd-concentration. This cutoff wavevector is related to a finite length of conformational change, shown in molecular dynamics (MD) simulation of filaments [61], or not would be open question. Thus enhanced rotation of higher concentrations in VH-mode is not distinguishable any more, due to the one slow-mode dominant relaxation. In general, the interpretation of two modes in both VV- and VH-mode are distinguished, according to our scattering geometry, as the fast mode is rather related to the ion-dissociated solvent acting on the parallel motions of charged-fd-rods, while as the slow mode is corresponding to the "twist" angle or the perpendicular motions of rod-rod interactions. This can be then regarded as "restoring" rotations with a unique spatial coherence length, which is an intriguing observation when the concentration is sufficiently high enough to carry the coupled motions of rotation to translation. As a result, the system is overdamped with a rotational degree of freedom exhibiting to a slowing down behavior, as well as ordered orientations of "domain" structure may be formed during a reorganization process [62].

VII. DYNAMIC COHERENCE LENGTH OF CHARGED CHIRAL FD-RODS

At a current lower ionic strength (of 0.032 mM), the aspect ratio of charged fd-rods is much reduced (as 16) due to an increased effective diameter, which is much lower than the aspect ratio (of 60-133) at high ionic strength (above 1 mM salt). The system sets in the isotropic-nematic transitions effectively to the lower concentrations. Moreover, chiral nature of the surface of fd-viruses plays a role to have a stronger 'twist' interaction when the concentration is increased, at a fully-nematic as a chiral-nematic phase. As soon as approaching the chiral-nematic phase concentration, enormous slowing down behaviors are exhibited in the microscopic

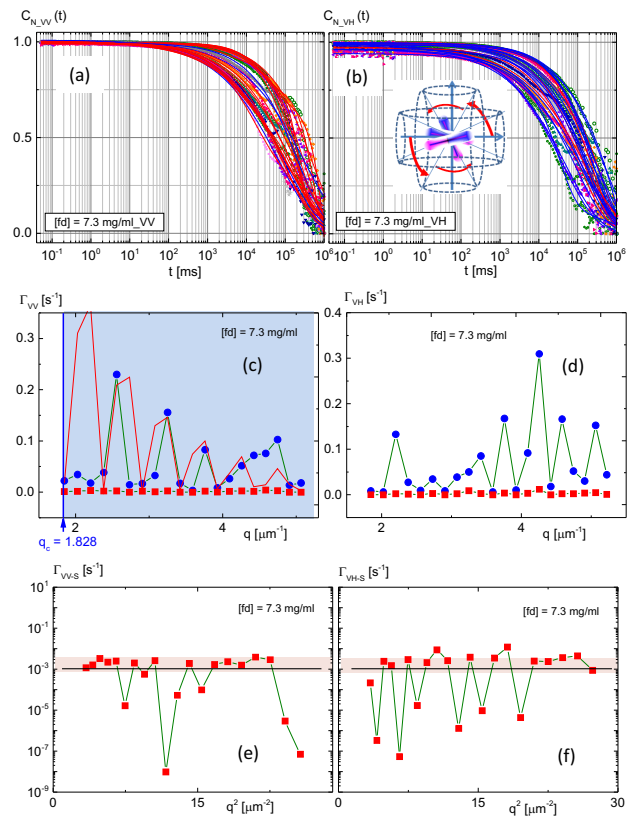


FIG. 19: The normalized correlation functions of (a) polarized VV-mode and (b) depolarized VH-mode for a hierarchical chiral mesophase (fd-concentration of 7.3 mg/ml). The inset is shown a brief illustration of the possible configuration. (c) and (d) are dispersion relations for fast- and slow-mode of polarized VV-scattering, and depolarized VH-scattering, and details of slow mode are shown in (e) and (f), respectively. The red line in the fast mode of (c) is depicted of the damping motion.

dynamics due to the existence of orientation texture.

From two dynamical modes, observed in overall dispersion relations of both polarized (VV) and depolarized (VH) light scattering, except only VV-scattering in an isotropic phase, fast mode is related to the thermal fluctuations of the parallel component, while as the slow mode is related to the perpendicular motions to the rods. The relaxation rates of a slow mode are typically shown to be as far low (as 100 times smaller). Also depending on the concentration, the role of a slow mode plays an interplay between rod-rod interactions via rotational motion and the "twist" elasticity. The distinctive cutoff wavevectors are found in the lower I-N binodal and a chiral-nematic phase concentration as the fast mode translational motions exhibiting to zero relaxation rates, i.e., relaxation time diverges. Furthermore, qualitatively different dispersion relations are observed in rotational motions, above a chiral-nematic phase concentration, while as the translational motions are much overdamped. Quite periodic relaxation rates are seen for the rotational motions with spacing of wavevector for a

hierarchical chiral-mesophases, which reveals an interesting aspect of relevant coherence length with a persistent length of fd-virus particle (as $2.26 \mu\text{m}$). As a result, the dynamic coherence length is estimated from $\xi = 2\pi/q_c$, where the cutoff wavevector q_c is measured in the soft mode of dispersion relations, plotted in **Figure 20a**, as a function of fd-concentration. Here the existence of a minimum coherence length at the lower I-N binodal concentration indicates that there is an enhanced 'twist' effect of charged chiral fd-rods, resulting from the reverse of an electrostatic interaction. Aligning effect increases by increasing a concentration up to a lower binodal, however above the lower I-N binodal concentration, the electrostatic repulsive interaction becomes stronger with a "twist" effect of charged fd-rods. The lowest line in **Figure 20a** indicates the value of bare length of fd-virus particle (as $0.88 \mu\text{m}$).

Finally, the brief outlook of possible spatial coherence length is illustrated in **Figure 20b**, as an increase of fd-concentration, such that the isotropic phase is shown with the equally probable rotations of two neighboring charged fd-rods that is not much different with the lowest limit of a persistent length of fd-virus itself (as $2.2 \mu\text{m}$). By upon entering a lower I-N binodal concentration, the coherence length becomes shorter as $1.24 \mu\text{m}$, where more aligned state is available, reducing the perpendicular gap among neighboring fd-rods. Interestingly, no spatial coherence length is observed at upper I-N binodal concentration in the fast mode of VV-scattering, but it is appeared in VH-scattering as $2.84 \mu\text{m}$, as a larger limit of a persistent length of fd-virus itself (as $2.8 \mu\text{m}$). At a chiral-nematic phase, slightly larger dynamic coherence length is observed as $1.54 \mu\text{m}$, indicated as the middle of the **Figure 20b**, where the charged fd-rods are twisted with rotations. By further increasing a concentration, larger correlation lengths are observed as $2.16 \mu\text{m}$ (for X^* -phase) and $3.44 \mu\text{m}$ (for H^* -phase), respectively. Consequently pronounced "twist" exist in the charged chiral fd-rods to keep larger spatial coherence length. In the case of non-chiral rods, the correlation length may differ at the I-N coexistence concentration due to either a lack of "twist" or stronger short-ranged attractions. The formation of chiral-nematic orientation textures of a finite pitch length also relies on the twist elastic modulus: Depending on the concentration, twist power parameter is varied with an intrinsic chiral interaction, distinguished by either X^* -(as lower) or H^* -phase (as higher) in hierarchical chiral mesophase concentration. Then the finite width of a wavevector suggests the dynamic coherence length with possible relevant length scales, such as (i) the persistence length of fd-virus as $2.2 - 2.8 \mu\text{m}$, (ii) the bare length of fd-virus (of $0.9 \mu\text{m}$), and (iii) the projections of an optical pitch length of chiral nematic-texture (of $5 - 10 \mu\text{m}$). For a lower concentration, there is a still separable diffusion between rotation and translation, however at higher concentration, the coupling of rotational motion to translation becomes dominant: As soon as approaching the

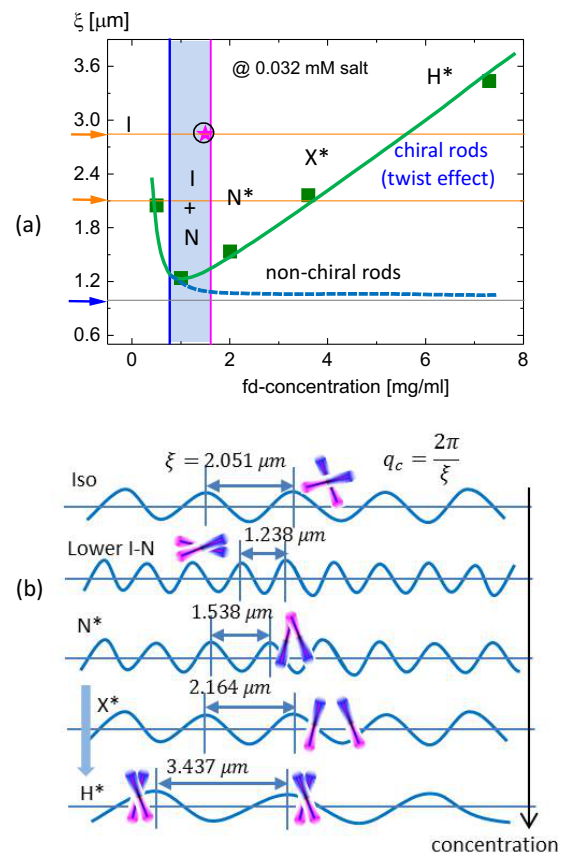


FIG. 20: (a) The result of a coherence length as a function of fd-concentration at a lower ionic strength (of 0.032 mM salt). There is a local decrease of the coherence length at approaching the lower I-N binodal concentration, as the minimum value of $\xi = 1.24 \mu\text{m}$, but it increase again above the binodal concentration. The lowest line is depicted as the bare length of fd-rod. (b) The brief scheme of possible configuration of spatial coherence lengths of collective soft mode of two interacting charged fd-rods: an isotropic, I, I-N binodal, I+N, a chiral-nematic, N^* , and hierarchical chiral-mesophases, as X^* , and H^* phase, as an increase of fd-concentration for a given low ionic strength.

chiral-nematic N^* -phase, the microscopic dynamics becomes enormously slower, due to the existence of orientational textures. Above the upper binodal concentration, not only the coupling of rotational motion to translation becomes dominant, but also the appearance of a minimal coherence length due to the increased "twist" interaction or the rotational motions of charged fd-rods. Therefore, a continuous rotation occurs vividly at higher concentration with a restoring "twist" deformation, such that translational motion is caged, but the slow mode is preserved by rotations of the whole cluster (or domains) in longer times. The spatial coherence length in the fast mode is then cooperated with the soft mode relaxation that persists in the orientation texture of charged chiral fd-viruses, reaching a new phase concentration.

VIII. CONCLUSIONS AND DISCUSSION

It is the first time that the collective soft mode is explored in a lyotropic system and shown in the dispersion relations of damping motions of charged chiral rods by means of small angle dynamic light scattering. The system is crowded suspensions of charged fibrous viruses (fd) at a low ionic strength (of 0.032mM salt), where the deformations of thick electric double layers are present. As an increase of concentration; microscopic dynamics are discussed for an isotropic, two I-N binodals, and a chiral-nematic phase, and two hierarchical chiral-mesophases. Chiral nature of the surface of fd-viruses plays a role to have a stronger 'twist' interaction when the concentration is increased, approaching a chiral-nematic phase. The continuous rotation occurs in the restoring "twist" deformation, such that translational motion is caged at a higher concentration, while as the slow mode

are mainly preserved in the rotations of the whole cluster (or domains) for much longer time variables. Most intriguing finding is the existence of a minimum coherence length at the lower I-N binodal concentration due to an enhanced "twist" effect of charged chiral fd-rods, as a consequence of reverse of the electrostatic repulsive forces. In near future, the "twist" effect of charged chiral fd-rods will be discussed by means of the optical pitch phase diagram as a function of an ionic strength and fd-concentration. The realistic microscopic description of two dynamical modes can be further described by including the motions of mobile ions attached to the charged fd-rods, either as the splay-bend or twist-bend elastic deformations. To check the fidelity of these specific elastic deformations of charged fd-rods, higher order Landau-Ginzburg equations should be considered in the kinetics of orientational order parameter.

-
- [1] I. Musevic, R. Blinc, B. Zeks, *The Physics of Ferroelectric and Antiferroelectric Liquid Crystals.*, Printed in Singapore by World Scientific Publishing Co. ISBN 981-02-0325-X, 2000.
- [2] J. Riseman, J.G. Kirkwood, *J. Chem. Phys.* **18** 512-516, 1950.
- [3] GCL. Wong, L. Pollack, *Annu. Rev. Phys. Chem.* **61** 171189, 2010.
- [4] S. Allison, C. Chen, D. Stigter *D. Biophys. J.* **81** 2558-2568, 2001.
- [5] RS. Dias, J. Innerlohinger, O. Glatter, MG. Miguel, B. Lindman, *J. Phys. Chem. B.* **109** 10458-10463, 2005.
- [6] JB. Hubbard, JA. Mccammon, *J. Chem. Phys.* **87** 4339-4343, 1987.
- [7] B. Robertson *J. Chem. Phys.* **95** 3873-3876, 1991.
- [8] M. Drifford, J-P. Dalbiez, *J. Phys. Chem.* **87** 5368-53753, 1984.
- [9] JP. Hansen, IR. McDonald, *Phys. Rev. A.* **11** 2111-2123, 1975.
- [10] P. Schofield, *Proc. Phys. Soc.* **88** 149-170, 1966.
- [11] R. Pecora, *Annu. Rev. Biophys. Bioeng.* **1** 257-276, 1972.
- [12] R. Pecora, *J. Nanoparticle. Research.* **2** 123-131, 2000.
- [13] TA. King, A. Knox, JDG. Mcadam, *Biopolymers.* **12** 1917-1926, 1973.
- [14] JM. Schurr, KS. Schmitz, *Biopolymers.* **12** 1021-1045, 1973.
- [15] EE. Maier, R. Krause, M. Deggelmann, M. Hagenbuechle, R. Weber, S. Fraden, *Macromolecules.* **25** 1125-1133, 1992.
- [16] JC. Thomas, GC. Fletcher, *Biopolymers.* **18** 1333-1352, 1979.
- [17] D. Lehner, H. Lindner, O. Glatter, *Langmuir.* **16** 1689-1795, 2000.
- [18] E. Loh, E. Ralston, VN. Schumaker, *Biopolymers.* **18** 2549-2567, 1979.
- [19] E. Loh, *Biopolymers.* **18** 2569-2588, 1979.
- [20] K. Zimmermann, J. Hagedorn, CC. Heuck, M. Hinrichsen, J. Ludwig, *J. Biol. Chem.* **261** 1653, 1986.
- [21] GJ. Thomas, B. Prescott, LA. Day, *J. Mol. Biol.* **165** 321-356, 1983.
- [22] C. Graf, M. Deggelmann, M. Hegenbuechle, H. Kramer, R. Kraus, C. Martin, R. Weber, *J. Chem. Phys.* **95** 6284-6289, 1991.
- [23] Th. Kirchhoff, H. Loewen, R. Klein, *Phys. Rev. E.* **53** 5011-5022, 1996.
- [24] B. Weyerich, BD. Aguanno, E. Canessa, R. Klein, *Faraday Discuss. Chem. Soc.* **90** 245-259, 1990.
- [25] J. Schneider, D. Karrer, JKG. Dhont, R. Klein, *J. Chem. Phys.* **87** 3008-3015, 1987.
- [26] LD. Landau, IM. Khalatnikov, *On the anomalous absorption of sound near the second order phase transitions.*, *Doklady Akademii Nauk SSSR* **96**, 469, 1954.
- [27] K. Kang, A. Wilk, A. Patkowski, JKG. Dhont, *J. Chem. Phys.* **126** 214501, 2007.
- [28] K. Kang, JKG. Dhont, *Soft Matter.* **9** 4359, 2013.
- [29] K. Kang K, JKG. Dhont, *Col. Poly. Sci.* **293** 3325-3336, 2015.
- [30] M. Doi, *Ferroelectrics.* **30** 247-254, 1980.
- [31] JKG. Dhont, K. Kang, *Soft Matter.* **10** 1987, 2014.
- [32] JKG. Dhont, K. Kang, *Soft Matter.* **11** 2893, 2015.
- [33] L. Onsager, *Phys. Rev.* **62** 558, 1942.
- [34] L. Onsager, *Ann. N.Y. Acad. Sci.* **51** 627, 1949.
- [35] M. Doi, *J. Polym. Sci.* **19** 229-243, 1981.
- [36] JG. Kirkwood, PL. Auer, *J. Chem. Phys.* **19** 19:281-283, 1951.
- [37] JE. Hearst, *J. Chem. Phys.* **38** 1062-1065, 1963.
- [38] PS. Russo, *Dynamic Light Scattering from Rigid and Nearly Rigid Rods in "Dynamic Light Scattering, the Method and Some Applications.*, W. Brown, ed., Oxford University Press: Oxford, 1993.
- [39] R. Cush, PS. Russo, Z. Kucukyavuz, Z. Bu, D. Neau, D. Shih, S. Kucukyavuz, H. Ricks, *Macromolecules.* **30** 4920-4926, 1997.
- [40] AJ. Masters, *Molecular Phys.* **56** 887-901, 1985.
- [41] BV. Derjaguin, VM. Mueller, YP. Toporov, *J. Coll. Int. Sci.* **53** 314-326, 1975.
- [42] ND. Gershon, I. Oppenheim, *J. Chem. Phys.* **59** 1337-1341, 1973.
- [43] DR. Bauer, JI. Brauman, R. Pecora, *Ann. Rev. Phys. Chem.* **27** 443-463, 1976.

- [44] R. Nossal, *Biophys. J.* **11** 341-354, 1971.
- [45] JP. Boon, R. Nossal, SH. Chen, *Biophys. J.* **14** 847-864, 1974.
- [46] SB. Dubin, G. Feher, GB. Benedek, *Biochemistry.* **12** 714-720, 1973.
- [47] M. Doi, T. Shimada, K. Okano, *J. Chem. Phys.* **88** 4070-4075, 1988.
- [48] MA. Tracy, R. Pecora, *Annu. Rev.Phys. Chem.* **43** 525-557, 1992.
- [49] H.C. van de Hulst, "Light Scattering by Small Particles", Dover Pub. Inc. N.Y. ISBN: 0-486-64229-3, 1957.
- [50] O. Glatter, *J. Appl. Cryst.* **12** 166-175, 1979.
- [51] O. Glatter, B. Hainisch, *J. Appl. Cryst.* **17** 435-441, 1984.
- [52] K. Kang, *Rev. of Sci. Instrum.* **82** 053903, 2011.
- [53] K. Kubota, B. Chu, *Biopolymers.* **22** 1461-1487, 1983.
- [54] D. Stigter, *Cell Biophys.* **11** 139-158, 1987.
- [55] AW. Fulmer, JA. Benbasat, VA. Bloomfield, *Biopolymers.* **20** 1147-1159, 1981.
- [56] SF. Schulz, EE. Maier, R. Krause, M. Hagenbuechle, M. Deggelmann, R. Weber, *J. Chem. Phys.* **92** 7087-7094, 1990.
- [57] T. Maeda, S. Fujime, *Macromolecules.* **18** 2430-2437, 1985.
- [58] SF. Schulz, EE. Maier, R. Weber, *J. Chem. Phys.* **90** 7-10, 1989.
- [59] J. Jorne, *J. theor. Biol.* **55** 529-532, 1975.
- [60] K. Kang, *Soft Matter.* **10** 3311, 2014.
- [61] Z. Qin, MJ. Buehler, *Phy. Rev. Lett.* **104** 198304, 2010.
- [62] IM. Lifshitz, *Sov. Phys. JETP.* **15** 939-942, 1962.